Archives of Biochemistry and Biophysics 565 (2015) 57–67

Contents lists available at ScienceDirect

Archives of Biochemistry and Biophysics

journal homepage: www.elsevier.com/locate/yabbi

The C-terminal region of the human p23 chaperone modulates its structure and function

Thiago V. Seraphim [a], Lisandra M. Gava [b], David Z. Mokry [c], Thiago C. Cagliari [c,d], Leandro R.S. Barbosa [e], Carlos H.I. Ramos [c,*], Júlio C. Borges [a,*]

[a] Institute of Chemistry of São Carlos, University of São Paulo – USP, São Carlos, SP 13560-970, Brazil
[b] Department of Genetics and Evolution, Federal University of São Carlos – UFSCar, São Carlos, SP 13565-905, Brazil
[c] Institute of Chemistry, University of Campinas – UNICAMP, P.O. Box 6154, Campinas, SP 13083-970, Brazil
[d] Institute of Biology, University of Campinas – UNICAMP, Campinas, SP 13083-970, Brazil
[e] Institute of Physics, University of São Paulo – USP, São Paulo, SP 05508-090, Brazil

ARTICLE INFO

Article history:
Received 23 September 2014
and in revised form 27 October 2014
Available online 10 November 2014

Keywords:
p23
p19
Hsp90
Sba1
Molecular chaperone

ABSTRACT

The p23 protein is a chaperone widely involved in protein homeostasis, well known as an Hsp90 co-chaperone since it also controls the Hsp90 chaperone cycle. Human p23 includes a β-sheet domain, responsible for interacting with Hsp90; and a charged C-terminal region whose function is not clear, but seems to be natively unfolded. p23 can undergo caspase-dependent proteolytic cleavage to form p19 ($p23_{1-142}$), which is involved in apoptosis, while p23 has anti-apoptotic activity. To better elucidate the function of the human p23 C-terminal region, we studied comparatively the full-length human p23 and three C-terminal truncation mutants: $p23_{1-117}$; $p23_{1-131}$ and $p23_{1-142}$. Our data indicate that p23 and p19 have distinct characteristics, whereas the other two truncations behave similarly, with some differences to p23 and p19. We found that part of the C-terminal region can fold in an α-helix conformation and slightly contributes to p23 thermal-stability, suggesting that the C-terminal interacts with the β-sheet domain. As a whole, our results suggest that the C-terminal region of p23 is critical for its structure–function relationship. A mechanism where the human p23 C-terminal region behaves as an activation/inhibition module for different p23 activities is proposed.

Introduction

The small acidic p23 protein is a chaperone highly abundant in eukaryotes and is involved in protein homeostasis. It is physically and functionally connected to systems working in protein transport, ribosome biogenesis, signaling, transcription activation, and chromatin remodeling [1]. Nevertheless, p23 is better known as an Hsp90 co-chaperone since it regulates the ATPase cycle and client protein release of the latter. p23 was initially described as participating in progesterone receptor complexes together with the Hsp90 chaperone machinery [2–4]. However, the emerging p23 interactome has shown that p23 is more than an Hsp90 co-chaperone, having its own hub connections independent of Hsp90 [1,5,6]. Approximately 25% of the Hsp90 and p23 interaction networks overlap, suggesting that p23 also plays several Hsp90-independent roles [6]. Indeed, p23 presents prostaglandin E3 synthase activity [7,8], which is dependent on the p23 casein kinase phosphorylation mediated by Hsp90-p23 binding [7], and is involved in the cell death program in a way independent of Hsp90 [9–11].

Human p23 is a protein with an N-terminal core containing a β-sheet structured domain and a C-terminal acidic tail [12,13]. The p23–Hsp90 interaction occurs through the β-sheet domain of p23, which is sufficient for its proper interaction [12,14,15]. Whereas the C-terminal tail is poorly characterized, the β-sheet domain is involved in binding partially unfolded client proteins and interacting with Hsp90 [13,14,16,17].

Hsp90 is considered as an important target for cancer therapies, since it also stabilizes oncogenic proteins and is up-regulated in malignant tumors and cells [18–20]. Albeit the Hsp90-p23

Abbreviations: AUC, analytical ultracentrifugation; CD, circular dichroism; DSC, differential scanning calorimetry; f/f_0, frictional ratio; MM, molecular mass; Rs, Stokes radius; s, sedimentation coefficient; $s_{20,w}$, s at standard conditions; $s^0_{20,w}$, $s_{20,w}$ at 0 mg/mL of protein; s_{sph}, maximum s for a non-hydrated globular protein; [Θ], residual molar ellipticity; $\langle\lambda\rangle$, spectral center of mass; Rg, radius of gyration; D_{max}, maximum dimension.

* Corresponding authors.
E-mail addresses: cramos@iqm.unicamp.br (C.H.I. Ramos), borgesjc@iqsc.usp.br (J.C. Borges).

http://dx.doi.org/10.1016/j.abb.2014.10.015
0003-9861/

complex is also related to cancer progression by regulating some pathways, p23 can also regulate the expression of some genes by itself, in an Hsp90-independent manner [21]. p23 can bind to the N-terminus of ATP bound Hsp90 [2,3] and stimulates Hsp90-client protein dissociation [22]. In yeast, interaction between the p23 ortholog (Sba1) and Hsp90 leads to Hsp90N-terminal domain dimerization [23–25]. The Hsp90-p23 interaction can be synthetically blocked by several Hsp90 inhibitors, such as geldanamycin (GA) and radicicol (RDC), thereby inhibiting the Hsp90 cycle [26] and directing client proteins to the degradation machinery [27,28]. Although not essential for yeast, *sba1* knock out strains are hypersensitive to these compounds, which can be rescued by expression of either yeast or human orthologs [14,29]. In addition, an Sba1 C-terminal truncation mutant confers significant resistance against Hsp90 inhibitors [14]. In mice, p23 is absolutely essential for embryogenesis, however, its precise role remains unclear [30]. Most studies have focused on the p23 β-sheet domain and its interaction with Hsp90 and have neglected other regions of the protein not involved in binding to Hsp90, reflecting a lack of fundamental understanding about p23 structure–function. Many functions of p23 have been attributed to its C-terminal tail, which is essential for its intrinsic chaperone activity [12–14], including its cooperative chaperone function with Hsp90 on the progesterone receptor maturation [12] and to promote functional telomerase complexes [31,32]. However, a C-terminal tail truncation does not inhibit the association of p23 and Hsp90, suggesting that it is not crucial for the p23–Hsp90 complex interaction [13,14]. The C-terminal region of p23 could function as a "fly casting" tail for the β-sheet domain holding client proteins in solution or to mediate interactions with protein partners [13,15]. The human p23 protein has been reported to be a CK2 kinase substrate, which regulates its prostaglandin E synthase activity by phosphorylating serine residues at the p23 C-terminal region [7]. Also, an *A. thaliana* p23 ortholog was found as being a CK2 substrate, and serine residues at the C-terminal region were predicted as potential phosphorylation sites [33].

The importance of the C-terminal tail of p23 has been further emphasized by the discovery that it can be specifically degraded by caspases 3 and 7 after Asp142, forming a 19 kDa degradation product (p19 or $p23_{1-142}$; Fig. 1) that is stable and functional in apoptotic cells and possesses smaller chaperone activity than p23 [9–11,32]. It has been suggested that p23 works as an anti-apoptotic factor and its C-terminal region holds an important role for p23 in regulation of apoptotic cells, either dependent or independent of Hsp90 [9,11,32]. Cleavage of p23 to form p19 occurs during endoplasmic reticulum stress-induced cell death, and the subcellular localization profiles of the two proteins are different, with p23 being mainly associated with the endoplasmic reticulum compartment, and p19 being predominantly detected as a cytosolic protein [34]. Unsurprisingly, p23 cleavage by caspases also leads to Hsp90 dysfunction which deregulates telomerase function by ubiquitination and degradation [32]. Although both p23 and p19 are able to interact with Hsp90, which indicates that the C-terminal tail is dispensable for this interaction, they do so in different manners [10,11,32]. The different constructs also may be responsible for controlling Hsp90 post-translational modifications, as serine phosphorylation is dependent on p23, and p19 promotes Hsp90 dephosphorylation [32]. Lastly, it was recently reported that gedunin, a natural compound, interacts with and inactivates human p23 as well as leads to p19 formation, via caspase activation, suggesting that gedunin may influence the p23 C-terminal conformation by interacting with the β-sheet domain [35]. Taken together, the p23 C-terminal region may act as a regulator of p23 function.

In order to address the function of the human p23 C-terminal tail, we performed *in vivo* yeast complementation assays using p23, p19 ($p23_{1-142}$) and two additional truncation mutants of its C-terminal region ($p23_{1-131}$ and $p23_{1-117}$) (Fig. 1). Additionally, we performed biophysical and biochemical characterization of human p23 and its truncation mutants pointing out the structure–function relationship of the p23 C-terminal region. Our findings are discussed in the context of the structure and function of the human p23 C-terminal tail and its role in interacting with client proteins.

Materials and methods

Yeast complementation assays

This study utilized two yeast strains; BY4741 as the wild-type (MATa *his3Δ1 leu2Δ0 met15Δ0 ura3Δ0*), and the isogenic knockout of the gene *sba1*, purchased from Open Biosystems, Inc., (YSC1021-552834). Strains were transformed with the desired plasmids as

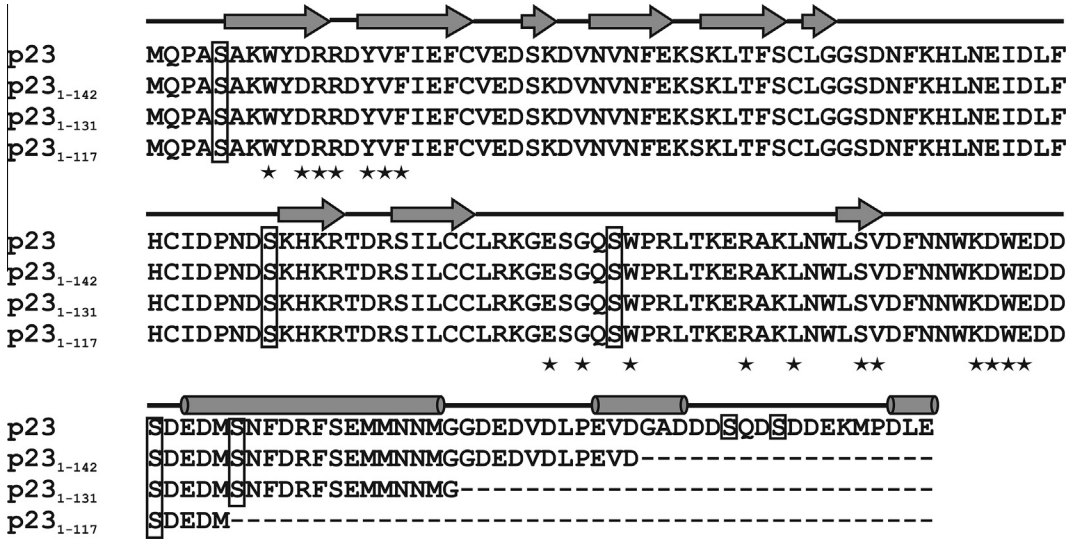

Fig. 1. Amino acid sequence of human p23 and mutants. Amino acid alignment of p23 and its C-terminal truncation mutants showing the secondary structure content based on the crystallographic structure (PDB ID: 1EJF) and the prediction of the amphipathic α-helix as predicted by the program Antheprot [36]. The amino acids involved with Hsp90 interaction are indicated by stars and the predicted phosphorylated Ser residues are inside the rectangles.

previously described [37], and 5–6 colonies were inoculated into Synthetic Complete media lacking uracil (SC-Ura) and allowed to grow at 30 °C for 24 h. After this time, the cultures were pelleted by centrifugation (3,220*g* × 10 min), washed twice with sterile ddH_2O, and then transferred to 50 mL SG-Ura medium (containing 2% galactose instead of 2% glucose) at 30 °C for 14–16 h. Following induction, cultures were standardized to OD_{600nm} 0.49 ± 0.01 in SG-Ura. Cultures were then treated differently, depending on the purpose of the experiment. Where RDC and GA were assessed, samples from cultures following standardization were serially diluted 1:10 in a 96-well plate and immediately spotted (2.5 μL) onto an SG-Ura plate containing either 50 μM GA, 100 μM RDC, or the appropriate amount of DMSO (control). For heat shock experiments, samples of standardized cultures were pretreated with 2.8% DMSO at 30 °C for 30 min, followed by 35 min at 37 °C. Aliquots were then removed and submitted to a lethal heat-shock treatment at 53 °C for 20 min, and immediately placed on ice and spotted onto SC-Ura plates as described above. Plates were incubated either at 30 °C for 2–5 days (heat-shock and GA plates) or 10 °C (RDC) for 2 weeks. All yeast experiments were repeated at least twice in triplicate from different yeast transformants.

Plasmid constructs

The cloned cDNA for human p23 was obtained from the IMAGE consortium (dBEST reference: 4704885) and subcloned into a pET28a expression vector (Novagen) using specific primers (data not shown). This strategy allowed the construction of the pET28a::hp23 vector which expresses the human p23 containing a 6xHis-tag peptide fused to the N-terminal region. The truncation mutants of the C-terminal region of p23 were built using the pET28a::hp23 vector as a template and standard PCR using specific primers for the introduction of a stop codon after the Asp142, Gly131 or Met117 codons, followed by subcloning, to generate pET28a::$hp23_{1-142}$, pET28a::$hp23_{1-131}$ and pET28a::$hp23_{1-117}$ expression vectors, respectively. All cloned sequences were checked by DNA sequencing.

All yeast expression plasmids were created by *in vivo* homologous recombination in yeast using a centromeric (low-copy) vector containing a URA3 marker and GAL promoter as previously described (SM640) [38,39]. In short, amplification of the gene of interest supplied by the vectors described above (for human p23), or by yeast genomic DNA (for Sba1), was carried out using the appropriate primers and recombination was facilitated by cotransforming yeast (strain BY4741) with the resulting PCR product and SM640 linearized with *EcoRI* and *XmaI* (New England Biolabs). The transformation mix was then plated onto SC-Ura solid media, and incubated at 30 °C for 2–3 days.

To identify clones with the correct DNA insertion, independent yeast colonies were inoculated into liquid SC-Ura medium and grown to saturation at 30 °C. Plasmid extraction was carried out by disruption with acid-washed glass beads (Sigma, G8772) coupled to a modified plasmid miniprep protocol (Qiagen). The extracted plasmids were reamplified in *Escherichia coli* (DH5α) and screened by restriction digest analysis, PCR amplification and finally, DNA sequencing. All clones contained the identical sequence to those for hp23 and sba1 available at NCBI database, except for the last amino acid of hp23 which encoded an aspartic acid in place of a glutamic acid residue in the plasmid for yeast expression.

Protein expression and purification

All recombinant proteins produced for purification were expressed in *E. coli* BL21(DE3). Cells were grown at 37 °C in LB medium containing 35 μg/mL of kanamycin to OD_{600nm} = 0.6–0.8, from which protein expression was induced with 0.4 mM isopropyl thio-β-D-galactoside (IPTG) at 30 °C. After 4 h of induction, cells were harvested by centrifugation for 10 min at 2,600*g*. Pellets were resuspended in 20 mM sodium phosphate (pH 7.4), 500 mM NaCl, 20 mM imidazole (15 mL/L of culture) and incubated with 5 U of DNase (Promega) and 30 μg/mL of lysozyme (Sigma) for 30 min on ice. The bacterial cells were disrupted by sonication and centrifuged at 20,000*g* for 30 min at 4 °C. The supernatant was filtered through a 0.45 μm membrane and submitted to Ni^{2+}-ion affinity chromatography in a HiTrap Chelating column. Proteins were eluted with 20 mM Sodium phosphate (pH 7.4), 500 mM NaCl, 500 mM imidazole buffer and incubated overnight at 4 °C with thrombin (Sigma) for His-tag cleavage (10 U/10–15 mg of protein). The protein purification polishing step was performed by size exclusion chromatography using a Superdex 200-containing column coupled to an Äkta Prime Plus system (GE Healthcare LifeSciences) using 25 mM Tris–HCl (pH 7.5), 100 mM NaCl, 5 mM β-mercaptoethanol buffer (herein referred to as p23 buffer). All purification steps were monitored by 15% SDS–PAGE. The protein concentration was determined by absorbance at 280 nm, using the calculated extinction coefficient for denatured proteins estimated by the Sednterp program (www.jphilo.mailway.com/download.htm).

Immunoblotting of p23 in yeast

Detection of recombinant human p23 expression in yeast was done by western blotting of yeast whole cell extracts prepared by post-alkaline extraction as described in [40]. Samples were pelleted and 5 μL of the supernatants were loaded onto a 12% SDS–PAGE and the proteins were transferred to a 0.45 μM nitrocellulose membrane (Whatman). A 1:350 dilution of the primary antibody against the N-terminus of p23 (Abcam #133186) and a 1:3000 dilution of the secondary antibody conjugated to HRP (Abcam # 6721) were applied. The bands were developed using the Supersignal® West Pico Chemiluminescent Substrate (Thermo Scientific) and analyzed by a digital imaging system (GE Healthcare ImageQuant™ LAS 4000).

Spectroscopy studies

Circular dichroism (CD) measurements were performed in a Jasco J-815 spectropolarimeter coupled to a Peltier-type temperature control system following standard procedures [41]. All experiments were performed in p23 buffer, with protein concentrations ranging from 5 to 40 μM and in 0.2 mm or 1 mm quartz cells. All CD data were normalized for molar residual ellipticity (MRE). Thermal-induced unfolding experiments followed by CD were performed with 1 mg/mL protein in a 1 mm quartz cuvette using a heating rate of 1 °C/min and data acquisition at 231 nm in 0.5 °C intervals. Tm, the temperature at the midpoint transition, was obtained by fitting the delta of signal data to a sigmoidal Boltzmann function.

Intrinsic fluorescence emission measurements were performed in an F-4500 Fluorescence Spectrometer (Hitachi) using a 1 × 0.2 cm pathlength cuvette with 2.5 μM protein in p23 buffer at room temperature. The excitation wavelength was 280 nm and fluorescence emission was measured from 300 to 420 nm. The data were analyzed by the maximum fluorescence emission wavelength (λ_{max}) and spectral center of mass (<λ>), as described by the following equation:

$$<\lambda>=\sum \lambda_i F_i / \sum F_i \quad (1)$$

where λ_I represents each wavelength observed, and F_i represents the fluorescence intensity at each wavelength.

Differential scanning calorimetry

The measurements of thermal-induced unfolding followed by Differential Scanning Calorimetry (DSC) were performed in a Nano DSC (TA Instruments). Measurements were taken at protein concentrations of approximately 1.0 mg/mL in p23 buffer without β-mercaptoethanol. Extensive dialyses were performed in all steps. The scan rate was 1.0 °C/min at the temperature range of 15–90 °C. The reversibility of thermal unfolding was tested by performing several consecutive up/down scans.

The experimental thermograms were collected using DSCrun software (TA Instruments) and fitted using NanoAnalyze software (TA Instruments), both supplied with the device. The baselines were calculated from the pre- and post-transition temperature regions. The apparent calorimetric enthalpy change of the unfolding transition (ΔH^{cal}_{app}) was calculated by integrating the area under the peak of the heat capacity of the unfolding transition (Cp^{trs}) using the following equation where T is the temperature in kelvin. Tm was estimated as the midpoint of transition.

$$\Delta H^{cal}_{app} = \int_{T1}^{T2} Cp^{trs} dT \quad (2)$$

Hydrodynamic characterization

Analytical size exclusion chromatography experiments (aSEC) were carried out using a Superdex 200 10/300 GL column coupled to an Äkta Prime Plus device and the elution profile of the samples was monitored by their absorbance at 280 nm. A volume of 100 μL of each sample, along with a Stokes radius (Rs) standard protein pool (Ferritin – 61 Å; γ-globulin – 48 Å; BSA – 36 Å; Ovalbumin – 30 Å; and carbonic anhydrase 24 Å, with all concentrations at approximately 1 mg/mL), were applied onto a p23 buffer pre-equilibrated column. The void volume of the column was determined by Blue dextran at 1 mg/mL. The elution volume of each protein was used to calculate the partition coefficient (k_{av}), by the following equation:

$$K_{av} = \frac{V_e - V_0}{V_t - V_0} \quad (3)$$

where V_t and V_0 are the total and the void volume of the column, respectively, and V_e is the elution volume of the protein. To determine the Stokes radii of p23 and its truncation mutants, a graph of the Rs as a function of the $-(\log k_{av})^{1/2}$ was constructed and fitted by linear regression analysis. From the angular and linear coefficient, the Rs of the proteins were calculated. The indirect molecular mass parameter was estimated from the dependence of the k_{av} and the log of the MM of the standard proteins. The software Sednterp was applied to estimate the hydrodynamic properties of p23, $p23_{1-142}$, $p23_{1-131}$ and $p23_{1-117}$ through their primary sequence: V_{bar} was 0.7098 mL/g, 0.7144 mL/g, 0.7154 mL/g and 0.7186, respectively. The Sednterp software was also employed to estimate the buffer viscosity ($\eta = 1.0185 \times 10^{-2}$ poise) and density ($\rho = 1.00307$ g/mL).

Sedimentation velocity experiments for p23 and the truncation mutants were performed in a Beckman Optima XL-A analytical ultracentrifuge (Beckman Coulter) in concentrations ranging from 0.15 to 1.00 mg/mL in p23 buffer, at 20 °C, 42,000 rpm (AN-60Ti rotor). Data acquisitions were performed at 234 nm and 241 nm for p23, 279 nm and 290 nm for $p23_{1-142}$, 290 nm for $p23_{1-131}$, and 235 nm and 240 nm for $p23_{1-117}$. The software SedFit (Version 12.52) [42] was applied in order to fit the absorbance *versus* cell radius data. The apparent sedimentation coefficients (s) were determined by the maximum of the peaks of the continuous c(S) distribution curves. The apparent s values were corrected to the standard sedimentation coefficient ($s_{20,w}$) and, the $s_{20,w}$ values at 0 mg/mL protein concentration ($s^0_{20,w}$) were obtained by linear regression of these values as a function of protein concentration [43]. The protein's MM as determined in the AUC was obtained by the SedFit program.

Small angle X-ray scattering experiments

Small angle X-ray scattering (SAXS) measurements were performed in the SAXS beam line at the Brazilian Synchrotron Light Laboratory (LNLS/CNPEM – Campinas/SP). The X-ray scattering data were acquired using a Pilatus bidimensional detector with an X-ray wavelength of 1.488 Å and the sample-to-detector distance ~1000 mm, which corresponds to the scattering vector range from $0.015\ Å^{-1} < q < 0.41\ Å^{-1}$, where q is the magnitude of the q-vector defined by $q = (4\pi/\lambda)\sin\theta$ (with 2θ as the scattering angle). The samples were measured in 1 mm pathlength mica cells and the scattering profiles were collected in 30 s frames. The proteins were prepared in p23 buffer at concentrations of approximately 1 and 2 mg/mL. The data acquisitions were obtained at 20 °C and at least two independent measurements were performed. SAXS curves were scaled to the intensity of the incident radiation and the sample's attenuation. The corrected buffer SAXS curves were subtracted from the samples' scattering. Concerning the data analysis, the SAXS curves were normalized to the protein concentration and data quality was inspected by the Primus program [44]. The GNOM program [45] was used to generate the particle distance distribution function – $p(r)$ – from the scattering curves. The $p(r)$ function furnishes information about the size and shape of the protein and is related to the probability of finding a pair of small scattering elements inside of the protein [46].

Chaperone activity experiments

Chaperone activity of p23 and its C-terminal truncation mutants was verified by the ability to prevent the aggregation of the model client proteins malic dehydrogenase (MDH) and luciferase (Luc) monitored by light scattering at 320 nm. Protein (p23, $p23_{1-142}$, $p23_{1-131}$ or $p23_{1-117}$) at 5 μM, was incubated with 1 μM of MDH or Luc at 42 °C for 5 h in 40 mM HEPES (pH 7.5) containing 5 mM KCl. Aggregation was monitored by absorbance at 320 nm in a microplate spectrophotometer Multiskan GO (Thermo Scientific).

Results

Yeast complementation assays

A yeast system involving Hsp90 inhibitors to monitor the function of the human p23 C-terminal tail was used, since a similar system had already been applied to investigate the functional domains of Sba1 [14]. All of the human p23 constructs expressed well in yeast and to relatively the same degree (Fig. S1 – Supplementary material), with mildly lower expression associated with $p23_{1-142}$, which was not enough to impart a difference in our *in vivo* complementation assays (see below). The antibody used in the immunoblotting was not observed to have cross-reactivity with recombinant or native Sba1, but did recognize recombinant human p23 purified from *E. coli* (data not shown).

Molarities of ansamycin compounds were used at threshold concentrations growth inhibition in the mutant (*sba1Δ*) strain. After two days in the presence of 50 μM GA, evidence of growth was observed in all of the strains expressing the human p23 constructs, with slightly lower cell confluency associated with the full-length p23 form (see Discussion). After 5 days, growth was observed in all of the strains, with a much higher confluency

associated with expression of the human p23 constructs (Fig. 2A, top panel). The growth profile in the presence of 100 μM RDC was identical to that of GA, with the exception that the compound had slightly lower growth inhibitive properties, as the results are best viewed in the first 1:10 dilution (Fig. 2A, lower panel). The wild-type strain, which carries Sba1 under its native promoter, grew less than the strains overexpressing Sba1 or p23, but was not as defective in its growth as the p23 null strains transformed with an empty vector. These results were dependent on the presence of the compounds, but not on the DMSO solvent (Fig. 2B). As previously described [14], expression of Sba1 complemented the growth defect observed in both the presence of GA and RDC (data not shown). These data indicate that the p23 and truncation mutants can rescue yeast *sba1Δ* strains from Hsp90 inhibitor hypersensitivity, suggesting that they are able to properly interact with yeast Hsp90.

We consistently observed an increase in thermotolerance to a lethal heat shock treatment in human p23 and Sba1 expressing yeast, and so therefore developed an assay to compare their different thermal protective qualities. Like in the presence of ansamycin compounds, the C-terminal p23 truncations and Sba1 imparted higher survival rates, but with little effect observed in the case of full-length p23. In fact, the degrees of thermal resistance for human p23 followed the order $p23_{1-142} > p23_{1-117} > p23_{1-131} > p23$, with the differences between $p23_{1-117}$ and $p23_{1-131}$ being more subtle (Fig. 2C). We also saw no evidence that this result is an artifact of increased endogenous levels of yeast chaperones (Hsp40, Hsp70, and Hsp104), except for Hsp90, which was equally elevated in all strains expressing hp23. Intriguingly, the wild-type strain consistently showed less survival to heat shock than the isogenic *sba1Δ* strain (see Discussion). Comparative quantities of yeast were present in each culture, since all were standardized to within 0.01 OD_{600nm}, and equal numbers of colonies were present on untreated control plates (Fig. 2D). These results led to the hypothesis that the deletion of the region between 143 and 160, as that proteolyzed *in vivo* by caspases, enhances the stress resistance effect of p23.

Protein expression and purification

Fig. 1 depicts the primary structure of human p23 and its C-terminal truncation mutants studied here with emphasis on the β-sheet folded domain and the C-terminal tail, the conserved residues involved in the interaction with Hsp90, and some p23 Ser residues, which are predicted to be phosphorylated using the NetPhos server [47]. Interestingly, four *in vivo* phosphorylation sites are reported in the human p23 sequence, of which two are located on the C-terminal tail (Ser 148 and Ser 151) [48]. The figure also illustrates a predicted amphipathic α-helix, as predicted by the program Antheprot [36], in the p23 amino acid sequence between Met117 and Met130. All proteins for purification were expressed in *E. coli* cells in the soluble fraction and in high quantities. The proteins were purified to homogeneity as judged by coomassie stained SDS–PAGE (Fig. S2 – Supplementary material), and all are recognized by an antibody specific to the p23 N-terminus (data not shown).

Human p23 and its C-terminal truncations have different secondary structure contents

In order to determine if the purified p23 constructs retained secondary structural contents after purification, and to elucidate any differences between them, all were assessed by CD spectropolarimetry (Fig. 3A). The human p23 CD spectrum presents an

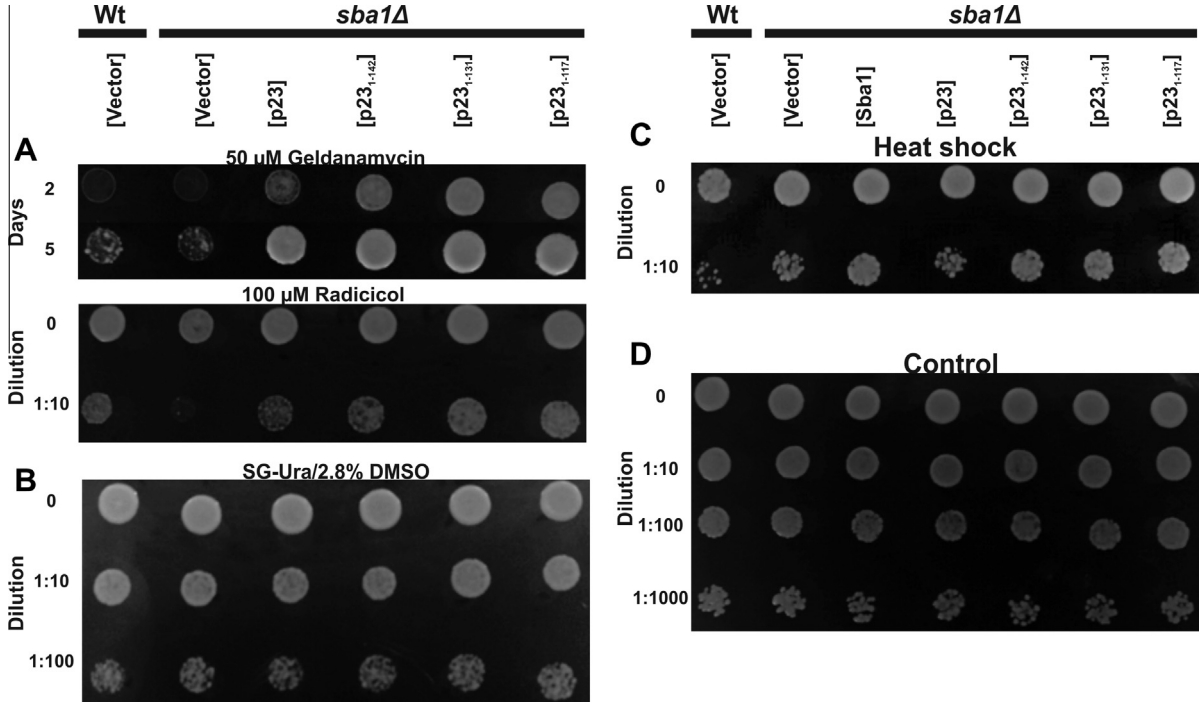

Fig. 2. Yeast complementation assays. (A) Standardized yeast cultures (A_{600}) plated on SG-Ura solid media containing 50 μM GA after 2 and 5 days at 30 °C (top panel), 100 μM RDC after two weeks at 10 °C (bottom panel), or solvent (2.8% DMSO) at 30 °C for 2 days (control, see panel B). All the human p23 constructs mitigated the growth inhibitory effects of the compounds, with the full-length human p23 exhibiting slightly less suppression. Therefore, p23 binding with Hsp90 was not impaired by the C-terminal truncations. (C) Thermotolerance of yeast expressing Sba1 and human p23 constructs relative to controls. Standardized yeast cultures (OD_{600nm}) were pretreated in 2.8% DMSO at 30 °C for 30 min followed by a mild heat shock at 37 °C for 35 min, and finally a lethal heat shock at 53 °C for 20 min and plated in 1:10 serial dilutions onto an SC-Ura agar plate. Yeast cells pretreated but not subjected to the lethal heat shock were also plated as a control (D). All p23 constructs, except the full-length p23, conferred thermotolerance as deemed by higher survival relative to an *sba1Δ* control strain containing an empty vector. Survival rates typically followed the order $p23_{1-142} > p23_{1-117} > p23_{1-131} > p23$.

unusual shape with a maximum at 231 nm, a shoulder at 218–220 nm and a minimum at 201 nm, the latter suggesting that the protein possesses unstructured regions [13,15]. The truncation mutant $p23_{1-142}$ has a smaller minimal CD signal at 231 nm than p23, and had a minimum at 205 nm. The $p23_{1-131}$ mutant spectrum indicates a minimum at 207 nm, suggesting loss of unstructured regions, or that it may contain some α-helical content that was not clearly observed in p23 and $p23_{1-142}$. On the contrary, the $p23_{1-117}$ CD spectrum shows a minimum between 203 and 216 nm, suggesting a dominant β-sheet content. Since an amphipathic α-helix was predicted at the C-terminal region of p23 (see Fig. 1), we obtained the peptides corresponding to the regions encompassing Ser_{118}-Gly_{131} and Gly_{132}-Asp_{142} and performed CD experiments which showed that both peptides were unstructured in the buffer conditions used (Fig. S3). However, at trifluoroethanol (TFE) concentrations higher than 10%, the peptide Ser_{118}-Gly_{131} showed CD signals at 208 and 222 nm, whereas, the peptide Gly_{132}-Asp_{142} had no propensity upon TFE titration in acquiring an α-helical structure (Fig. S3).

All purified proteins showed a positive CD signal at 231 nm, which is usually related to side chain conformations of aromatic amino acids that form a compact cluster, which is a characteristic of p23 proteins [13]. Therefore, this may be considered a parameter related to tertiary structure. The $[\theta]$ at 231 nm exhibited by $p23_{1-117}$ and $p23_{1-131}$ was comparatively 3–4 times higher than that observed for p23 (Fig. 3A), while this signal was less intense for $p23_{1-142}$, although still higher than p23. All p23 proteins studied here contain 5 tryptophans, 2 tyrosines and 7 phenylalanine residues (with the exception of $p23_{1-117}$, which has 5 phenylalanines) in their sequences. Many of these aromatic residues are located within a β-sheet domain and form a cluster, as observed in the crystallographic structure [12].

We applied the intrinsic emission fluorescence technique for the purpose of monitoring and comparing the environment in which the tryptophan residues are located in the β-sheet folded domain. The direct inspection of the emission fluorescence spectra (Fig. 3B) suggested that these residues are located in similar environments in p23 and in the truncation mutants since the λ_{max} observed for all proteins was approximately 337 ± 1 nm and the $<\lambda>$ values were calculated to be 346 ± 1 nm.

Taken together, both the CD and intrinsic emission fluorescence data suggested that p23 and the C-terminal truncation mutants were well folded proteins. Additionally the CD experiments indicated that $p23_{1-142}$ harbors a different secondary structure compared to p23 and its smaller truncation mutants. Furthermore, we found that the peptide Ser_{118}-Gly_{131} had a propensity to adopt an α-helical structure that depends on the formation of non-local contacts, thereby suggesting the possible existence of an amphipathic α-helix at the C-terminal of p23, $p23_{1-142}$ and $p23_{1-131}$.

All p23 proteins are elongated monomers in solution

It is an open question if p23 is a dimer in solution since it can form an aberrant dimer through a disulphide bond [12,49,50]. To shed light on this question, aSEC experiments were performed with p23 proteins (Fig. S4 – Supplementary material). The elution profiles recorded for p23 and $p23_{1-142}$ (Fig. S4A – Supplementary material) were related to twice the predicted MM for monomeric non-hydrated globular forms of p23 (Table 1). Interestingly, both $p23_{1-131}$ and $p23_{1-117}$ eluted with similar profiles and were also related to monomeric non-hydrated globular forms (Fig. S4A – Supplementary material). The calculation of the Stokes radii allowed estimates of the frictional ratio (f/f_0) (Fig. S4B – Supplementary material – Table 1) and revealed that p23 and $p23_{1-142}$ had an elongated shape in solution, whereas, $p23_{1-131}$ and $p23_{1-117}$ were less elongated.

To further investigate the hydrodynamic properties of p23 and its C-terminal truncation mutants, all four proteins were characterized by means of AUC experiments. Fig. S5 (Supplementary material) represents the c(S) distributions of all p23 proteins (at 1.0 mg/mL) indicating that they behave as homogeneous solutions in the tested conditions. In order to avoid interferences caused by the solution viscosity and molecular crowding [43], we determined the $s^0_{20,w}$ (Fig. 4A) resulting in values between 1.8 and 2.1 S (Table 1). These values suggested that p23 and the truncation mutants behave as monomers in solution, which is further supported by estimation of the MM by the SedFit program (Table 1). Furthermore, the f/f_0 estimated by the SedFit program implies that p23 conveyed a more elongated profile than $p23_{1-142}$, which was slightly elongated, while $p23_{1-131}$ and $p23_{1-117}$ had an even less elongated shape. These data also indicate that the p23 C-terminal region is responsible for conferring an elongated shape to p23.

The p23 C-terminal truncation reduces the dimension of p23

Fig. S6A (Supplementary material) shows the normalized SAXS curves of p23 and its truncation mutants, which are vertically shifted for clarity. The SAXS curves of p23 and the truncation mutants displayed linearity in the Guinier region (Fig. S6B), which provided evidence for the monodispersity of the protein samples

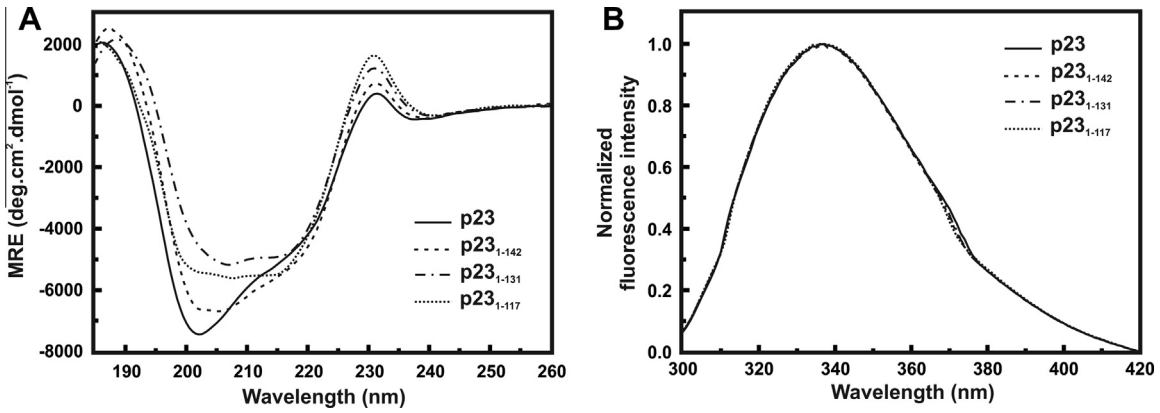

Fig. 3. Human p23 and mutants were purified containing rich secondary structures. (A) MRE of p23 and the truncation mutants obtained by CD showing that all proteins have diverse secondary structure content. The positive band at 231 nm comes from a cluster of aromatic amino acid residues and is related to the tertiary structure (see text for details). (B) Intrinsic fluorescence emission spectra of p23 and truncation mutants showing λ_{max} and $<\lambda>$ at about 336 nm and 346 nm, respectively (Table 1). Altogether, these data show that p23 and its truncation mutants are well-folded.

Table 1
Summary of the hydrodynamic and structural data of p23 and mutants.

Property	Technique	Protein			
		p23	$p23_{1-142}$	$p23_{1-131}$	$p23_{1-117}$
MM	Predicted	18.84	16.88	15.69	14.03
(kDa)	AUC	21 ± 1	20 ± 1	18 ± 1	15 ± 1
	aSEC	51 ± 4	34 ± 3	24 ± 2	22 ± 2
$s^0_{20,w}$ (S)	Predicted¤	2.79	2.55	2.42	2.21
	AUC[a]	1.93 ± 0.05	1.89 ± 0.05	1.85 ± 0.05	1.82 ± 0.05
Rs (Å)	Predicted[b]	17.4	16.8	16.4	15.8
	aSEC	31 ± 1	27 ± 1	23 ± 1	22 ± 1
f/f_0	AUC[c]	1.68 ± 0.06	1.45 ± 0.02	1.37 ± 0.03	1.34 ± 0.01
	aSEC[d]	1.78 ± 0.05	1.61 ± 0.05	1.40 ± 0.06	1.39 ± 0.06
Rg (Å)	SAXS	24.7 ± 0.3	20.9 ± 0.5	19.2 ± 0.3	19.2 ± 0.1
D_{max} (Å)		98 ± 3	83 ± 3	70 ± 1	67 ± 6

[a] Data extrapolated for water, 20 °C and 0 mg/mL protein.
[b] Values predicted as globular monomers in water and 20 °C (predicted by the Sednterp software).
[c] Calculated by SedFit software from the sedimentation velocity data.
[d] Data obtained using the Stokes equation for proteins of known Rs (predicted by the Sednterp software).

without any apparent protein aggregation. The radius of gyration (Rg) of the proteins was calculated and suggested that p23 is larger than $p23_{1-142}$, which in turn is larger than $p23_{1-131}$ and $p23_{1-117}$, as expected. The latter two proteins had similar Rg values (Table 1).

A more detailed analysis of the low-resolution structures of p23, $p23_{1-142}$, $p23_{1-131}$ and $p23_{1-117}$ was performed by generating the $p(r)$ distribution functions (Fig. 4B). The $p(r)$ curves suggested that all four proteins share some similarities, such as the $p(r)$ maximum position, which was ~25 Å for all studied protein constructs (Fig. 4B). Nevertheless, it should be noted that there were also some differences among the $p(r)$ functions, specifically concerning the protein maximum dimension, D_{max}. Notably, $p23_{1-117}$ and $p23_{1-131}$ showed some structural similarities, whereas p23 and $p23_{1-142}$ were clearly distinct. The $p(r)$ shape of all proteins implied their elongated shape, indicating that p23 had larger dimensions than $p23_{1-142}$, while $p23_{1-131}$ and $p23_{1-117}$ had smaller dimensions (Table 1). The C-terminal flexibility of the proteins was evaluated by means of the Kratky plot that, surprisingly, showed similar curve shapes suggesting that all proteins had similar flexibility, despite deletion of the C-terminal region (Fig. S6C). In addition, the $p(r)$ function resembles that found for randomly distributed homogeneous anisometric particles. In summary, p23 and $p23_{1-142}$ revealed a more elongated shape as compared to $p23_{1-131}$ and $p23_{1-117}$, which was in agreement with the aforementioned hydrodynamic experiments. Furthermore, the SAXS experiments showed that the structures of p23, $p23_{1-142}$ and $p23_{1-131}$/$p23_{1-117}$ were dissimilar, in particular concerning the protein D_{max}.

The p23 C-terminal tail stabilizes the β-sheet core

In order to address how the p23 C-terminus affects the stability of the protein, we took advantage of the CD signal at 231 nm and conducted thermal stability experiments using p23 and its truncation mutants. This CD signal is related to the aromatic amino acid cluster, therefore transitions involving this signal could be related to the p23 β-sheet core. Fig. 5A represents the delta of the CD signal recorded at 231 nm (Fig. S7 – Supplementary material), in order to allow inflexion curve comparisons, and allowed calculating the Tm for each thermal transition (Table 2). Although the differences in Tm were small from one deletion to the next, the overall stability decreased as the deletion of the C-terminus increased.

We also explored the thermal-induced transition of p23 and its truncation mutants by DSC which yields overall thermal stability information (Fig. 5B). In spite of the irreversibility of the thermal induced unfolding, we analyzed the thermal-induced unfolding transition to extract both Tm and ΔH^{cal}_{app}. Based on the Tm values, as well as those of ΔH^{cal}_{app} of the thermal transition (Table 2), we can observe that p23 was the most stable form studied here, while $p23_{1-117}$ was the least stable, once again showing that the overall stability is inversely proportional to the length of the C-terminal deletion. Based on CD and DSC thermal stability results, we can conclude that the p23 C-terminal tail interacts in a subtle way with the β-sheet core and modestly stabilizes it.

The C-terminal truncations impair the intrinsic chaperone activity of p23

To investigate the functional properties of p23 and its mutants, as well as the influence of the C-terminal region in its activity, aggregation protection experiments were performed using MDH (Fig. 6A) and Luciferase (Fig. 6B) as client proteins. At a 5:1 molar ratio, p23 almost completely suppressed the aggregation of MDH, whereas $p23_{1-142}$ prevented aggregation to approximately 50%. However, $p23_{1-131}$ and $p23_{1-117}$ likely co-aggregated with MDH, as deemed by an increase in the aggregation rate of approximately 50% (Fig. 6C). Although p23 was less efficient at preventing luciferase aggregation (Fig. 6D), it was still nonetheless possible to detect the same chaperone behavior as that observed for the MDH experiments, with the exception that $p23_{1-142}$ was deemed to prevent

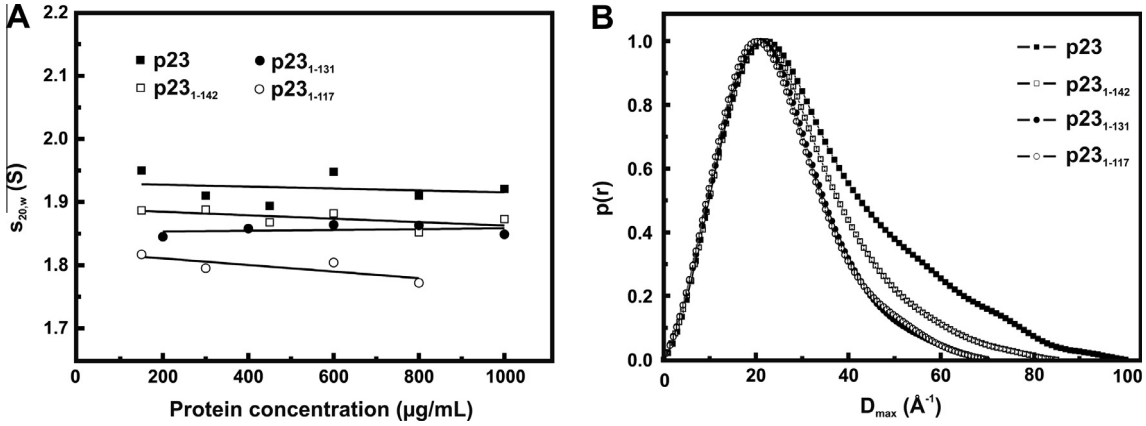

Fig. 4. Hydrodynamic and SAXS studies of p23 and truncation mutants suggest the proteins have elongated shapes, which are similar, but dimensions are variable. (A) Determination of the $s^0_{20,w}$ of p23 and its truncation mutants by linear regression analysis of $s_{20,w}$ (from Fig. S5 – Supplementary material). aSEC and AUC data showed that proteins had an elongated shape as follows p23 > $p23_{1-142}$ > $p23_{1-131}$ > $p23_{1-117}$. (B) Particle distance distribution function – $p(r)$ – from SAXS showing that p23 is larger than $p23_{1-142}$, which is more elongated than $p23_{1-131}$ and $p23_{1-117}$, which themselves in turn have similar dimensions.

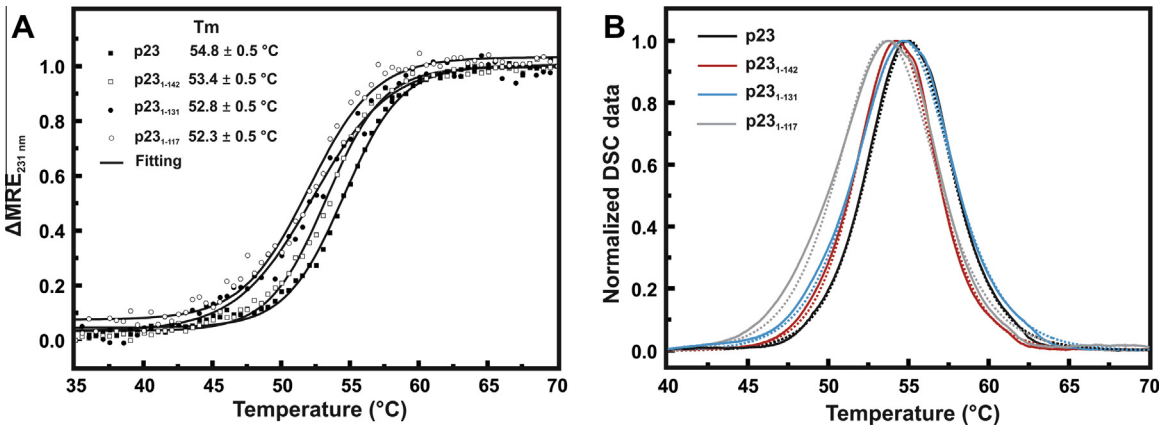

Fig. 5. Thermal-induced unfolding measurements of human p23 and truncation mutants indicate their different thermal stabilities. (A) Thermal-induced unfolding was followed by the MRE-signal at 231 nm (raw data is in Fig. S7), which is related to changes in the tertiary structure. Tms, the midpoint of the transition, were estimated by fitting with a sigmoidal Boltzmann function yielding values of 54.8, 53.4, 52.8 and 52.3 °C (errors are ±0.5 °C) for p23, p23$_{1-142}$, p23$_{1-131}$ and p23$_{1-117}$, respectively. (B) p23 and its truncation mutants were also submitted to DSC experiments. The figure shows the first scan of the heat capacity after subtraction of the buffer scanning and baseline treatment. Each Tm was estimated from the peak of the transition as well as the ΔH^{cal}_{app} by application of Eq. (2) giving values of 55.3, 54.4, 54.7 and 53.6 °C (errors are ±0.5 °C) for p23, p23$_{1-142}$, p23$_{1-131}$ and p23$_{1-117}$, respectively. The dotted lines represent the DSC data fitting. See text for details.

Table 2
Summary of the stability data observed in p23 and the mutants.

Property	Technique	Protein			
		p23	p23$_{1-142}$	p23$_{1-131}$	p23$_{1-117}$
Tm (°C)	CD$_{231\ nm}$[a]	54.8 ± 0.5	53.4 ± 0.5	52.8 ± 0.5	52.3 ± 0.5
	DSC	55.3 ± 0.2	54.4 ± 0.1	54.7 ± 0.2	53.6 ± 0.1
ΔH^{cal}_{app} (kcal/mol)	DSC	123 ± 1	123 ± 6	103 ± 5	98 ± 8

[a] Data estimated by sigmoidal fitting of the thermal-induced unfolding curves. Tm, temperature at the midpoint of the transition.

luciferase aggregation to the same degree than full-length p23. Therefore, the C-terminal region retains an essential role in the intrinsic chaperone activity of p23, especially in the region between residues 132 and 160 of the protein.

Discussion

p23 has been extensively studied by several strategies and numerous functions are attributed to it [1,5]. In spite of the aforementioned available information, the overall structure–function relationship is not fully understood [14] mainly concerning the role of the acidic C-terminal tail. In order to understand the p23 C-terminal function, we took advantage of the fact that human p23 expression in yeast rescues the sensitivity of an *sba1* knockout strain to Hsp90 inhibitors, and that this system had been used before to probe the functional domains of Sba1 [14,29]. We observed that p23 and all the truncation mutants conferred resistance to RDC and GA in Sba1 null cells. These results indicate that the p23 β-sheet domain, and not the C-terminal region, is responsible for interaction with Hsp90, and is consistent with data from previous studies [13,14]. Interestingly, the full-length p23 conferred slightly less resistance than the truncation constructs, and this was not due to differential expression levels. Although the reason for this is outside the scope of this study, it is consistent with a previous report that investigated the β-sheet domain (1–130) of Sba1 in the presence of GA and RDC compared to wild-type, and found that expression of solely this domain consistently complemented better than the full-length wild-type protein [14]. Hence, yeast and human p23 are behaving identically in the presence of these compounds.

Nonetheless, we determined that expression of different p23 constructs confer different degrees of thermotolerance. As with the previous results concerning the C-terminal truncation of Sba1 [14], p23$_{1-142}$, p23$_{1-131}$, and p23$_{1-117}$ increased survival to heat shock, but to different degrees (p23$_{1-142}$ > p23$_{1-117}$ > p23$_{1-131}$). We did not observe any obvious effect with full-length p23 under these conditions, despite slightly elevated expression levels in some experiments. As mentioned above, the differential survival rates were not due to other chaperone expression levels, including Hsp90 which was expressed at a higher, but similar, level in all p23 expressing strains. Curiously, the peptide corresponding to the p23 region encompassing Gly$_{132}$-Asp$_{142}$ showed thermal-induced structuration (Fig. S8), supporting conformational changes as a possible cause for the better performance of p23$_{1-142}$, but such hypothesis needs additional investigation to be further supported. Although higher survival rates for the p23$_{1-117}$ construct may seem counterintuitive, it is interesting to note that the yeast Sba1 is involved in a large network of *in vivo* interactions, which are both dependent and independent of Hsp90 [6]. Therefore, we suggest that upon heat shock, Hsp90 independent p23 interactions were differentially harmed by the p23 C-terminal truncations. Altogether, the complementation results promptly suggested that the p23 C-terminal region had an important role in the function of the protein, mainly considering its intrinsic chaperone activity and the *in vivo* functions annotated for p23$_{1-142}$.

Encouraged by our *in vivo* results, we decided to pursue *in vitro* studies with purified components in order to deepen the understanding of the roles of the p23 C-terminal tail. We obtained recombinant hp23 and three truncated C-terminal mutants with high purity, folded, and as monomers. Interestingly, although all proteins appeared to be well packed as seen by the CD signal at 231 nm and intrinsic fluorescence emission, it is interesting to note that the p23 characteristic CD signal at 231 nm increased even though the p23 C-terminal region was deleted. These results indicate that the p23 C-terminal region induces some structural changes near this CD chromophore environment in the β-sheet domain, that when truncated disturbs the CD signal intensity at 231 nm. Similar data have also been reported by at least two other groups studying human p23 [13,15]. Therefore the β-sheet folded domain is not an independent structure of the C-terminal tail. In addition, all proteins have different CD spectra, suggesting the influence of the C-terminal tail on the overall conformation of the protein. It worth noting the propensity of the Ser$_{118}$-Gly$_{131}$ segment to form an α-helical structure, which could be transient. However, it is not clearly observed by CD in the proteins studied here, since they have a higher amount of disordered structure

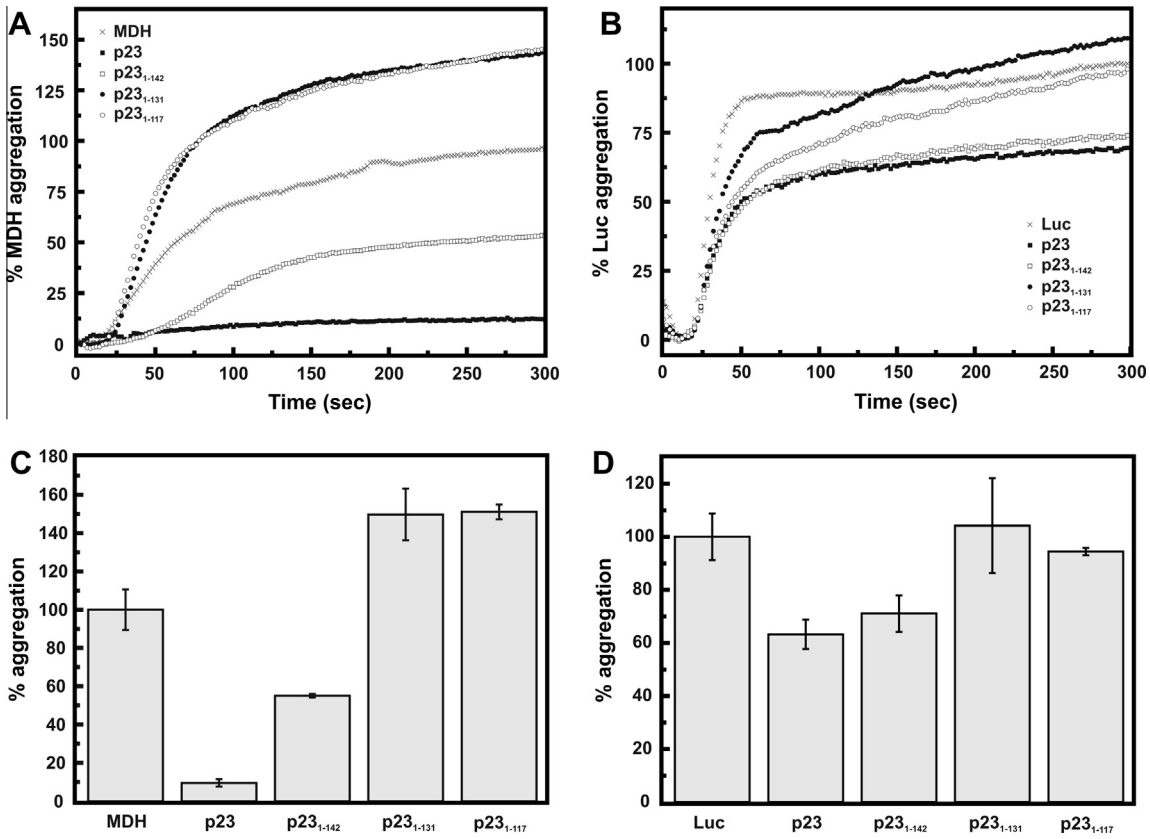

Fig. 6. Chaperone activity of human p23 is dependent on the length of the C-terminus. Prevention of client protein aggregation using (A–C) malic dehydrogenase (MDH) and (B–D) luciferase (Luc) as model client proteins. Both experiments were performed at the molar ratio of 5 μM p23 protein construct to 1 μM of model client protein. C–D represents the percent of aggregation (relative to the control) after 300 s (n = 3). The full-length protein was more efficient at preventing aggregation of MDH than $p23_{1-142}$, while both p23 and $p23_{1-142}$ were capable of preventing luciferase aggregation to the same degree. Both $p23_{1-131}$ and $p23_{1-117}$ either co-aggregated with the client proteins, or did not prevent aggregation. These results indicate that the C-terminal region has an essential role in the chaperone activity of human p23.

and a positive signal at 231 nm, which might mask their α-helical signals within their respective CD spectra.

The SAXS data obtained for p23 and the truncation mutants suggested that they were elongated monomers in solution and that the C-terminal region was partially responsible for the highly elongated shape of p23 and $p23_{1-142}$. Intuitively, the C-terminal truncation progressively reduced this p23 dimension, as observed in $p23_{1-142}$, followed by $p23_{1-131}$ and $p23_{1-117}$. The latter two had similar dimensions and suggested that either the p23 region encompassing Ser_{118}-Gly_{131} was likely less flexible than in the complete p23, or compacted within the β-sheet core domain, probably as an amphipathic α-helix. Furthermore, the Kratky plots of all p23 proteins have similarly shaped curves, suggesting that all of them had similar compactness. Interestingly, the C-terminal region of hp23 is promptly degraded by proteinase K leading to the formation of a stable fragment covering the p23 sequence of 1–130 [13], suggesting that the residues in the region between 115 and 130 adopt a folded structure.

Our thermal-induced unfolding experiments showed that the overall truncations of the C-terminal tail led to progressive reductions in the protein stability, suggesting that the C-terminal region contributes, in some way, to the p23 β-sheet thermal stability. Therefore, the p23 C-terminal tail could not be completely disordered and flexible, a result that is in contrast to a previous report that suggests that it constantly behaves as a "fly casting" [15]. The most likely explanation for this arises from the sequence between amino acid residues Glu_{115} and Met_{130}, in which secondary structure prediction analysis indicates the potential presence of an amphipathic α-helix structure, in this region that could interact with the p23 β-sheet folded domain, a suggestion that is corroborated by our CD and TFE titration. The interaction of this amphipathic α-helix may be dynamic and interact in a part of its lifetime with the β-sheet domain, since it may be influenced by the C-terminal region dynamics that follows. Also, the C-terminal region encompassed by the residues 142–160 could make some additional contacts with the β-sheet core domain, since p23 showed slightly increased thermal-stability in the CD experiments. Based on the structural and stability experiments, we propose that the p23 C-terminal region is, in some way, folded and/or subtly interacts with the β-sheet core domain in such a way that increases the p23 dimensions with a concomitant increase in its thermal stability and modifications in the CD signal at 231 nm.

It has been shown that p23 possesses intrinsic chaperone activity [12,13,16,17], however the exact roles of the p23 C-terminal region remain unknown. In our hands, p23 was able to prevent MDH client protein aggregation with higher efficiency than $p23_{1-142}$, whereas both prevented aggregation of luciferase to relatively the same degree. In contrast, $p23_{1-131}$ and $p23_{1-117}$ were not only defective in preventing protein aggregation, but seemed to co-aggregate with the client proteins. Therefore, the truncation of the region after the predicted amphipathic α-helix completely abolishes p23 chaperone activity, and the importance of the C-terminal region encoded between residues 142 and 160 in preventing protein aggregation is client protein dependent. Taken together, the chaperone activity of p23 is not limited to its β-sheet core domain, but also depends on a major part of the C-terminal tail. While this may seem partially in contrast to our *in vivo* yeast thermotolerance results, it is important to consider that the

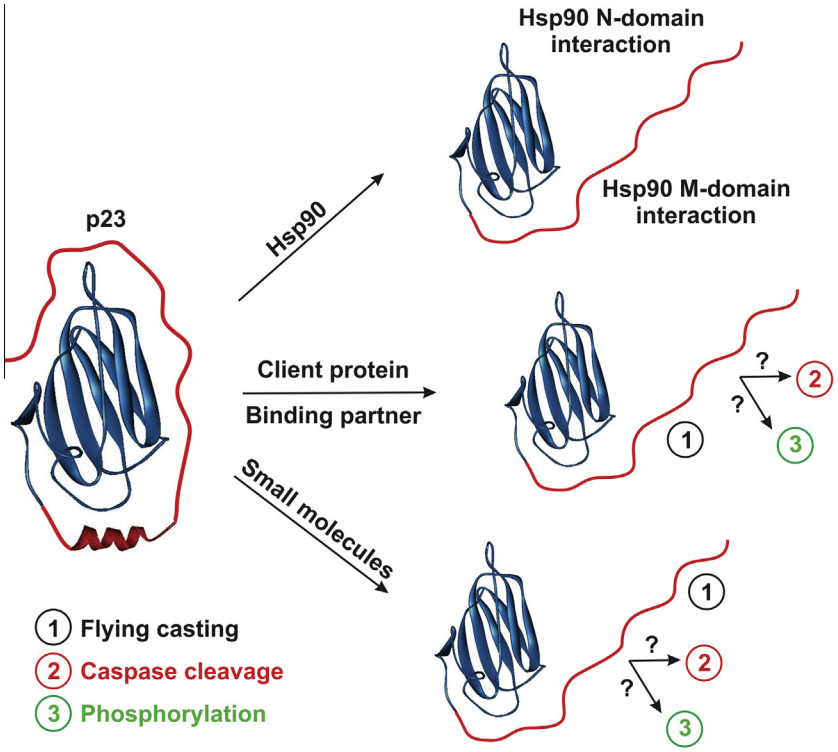

Fig. 7. Model for p23 mode of action. The β-sheet core of p23 interacts with the amphipathic α-helix and with the C-terminus by means of subtle contacts. The association of the p23 β-sheet core with Hsp90, client proteins/interacting partners or small molecules, such as gedunin, should disturb the soft interaction of the p23 C-terminal tail on the β-sheet core. Once the p23 C-terminal tail is released, it could allow additional interactions with the M-domain of Hsp90, or could act as a fly casting (1), recruiting interacting partners or even serve as a substrate for caspase cleavage (2), generating the p19 cleavage product, or serve as a substrate for phosphorylation (3).

purified proteins from *E. coli* lack any post-translational modifications. In addition, we used model client proteins for performing this *in vitro* analysis. The native interactions between p23 and other proteins in this network may depend upon specific post-translational modifications, or other factors (i.e. interaction with Hsp90) in order to correctly execute their functions. Importantly, this functional evidence further reinforces the idea that p23 and its p19 caspase-cleavage product have dissimilar biochemical properties.

Based on these experimental results, we believe that the human p23 C-terminal region may function as an activation or inhibition module that regulates the activity of p23 (Fig. 7). Inhibition modules are frequently intrinsically disordered regions of proteins, which allow several regulatory mechanisms [51]. The p23 dependence on the C-terminal tail for its intrinsic chaperone activity, which is related to the p23 β-sheet domain [12,13], suggests that it can assume a disordered conformation [15]. On the contrary, the ability of the C-terminal region to modify thermal stability of the p23 β-sheet domain suggests that it should be released from the β-sheet core domain after interaction with a client protein or a binding partner [15], Hsp90 [25], and/or small molecules [35], since p23 has prostaglandin E3 synthase activity [7,8]. It is well documented that the C-terminal region is not essential for modulating Hsp90 function [12,14,15], and the current study provides further proof of this. Nevertheless, Karagoz et al. [50] suggested that the interaction between Hsp90 and p23 occurs cooperatively, and that the p23 C-terminal tail may interact with the middle domain of Hsp90, resulting in additional conformational changes.

The p23 C-terminal tail seems to encode other functions for human p23. It can be cleaved by caspases 3 and 7 forming the stable p19 ($p23_{1-142}$) product that is involved in apoptosis [9,11] and regulates Hsp90 dephosphorylation [32], while full-length p23 has an anti-apoptotic action [9,11,32]. This evidence emphasizes the importance of the C-terminal region in regulating the various activities of p23. In addition, the p23 C-terminal tail contains two target residues for phosphorylation [48], which are not present in the p19 form. In all of these cases, free p23 should maintain its C-terminal region in close contact with the β-sheet domain. When one of those binding partners interacts with p23, the C-terminal tail may be released and assume disordered conformations acting as a "flying casting", or as a target region for protein partner recruitment or modifications. For example, Song and co-workers [52] describe the PXLE motif at the C-terminus of p23 as a recruitment site for partners involved in the Hsp90 chaperone machinery.

Taken together, we propose a model, based on our results and that of others, which summarizes the p23 C-terminal tail mechanism of action in the modulation of p23 (Fig. 7). In this model, the β-sheet core of p23 interacts with the amphipathic α-helix and the extremity of the C-terminal tail by means of subtle contacts. These contacts could be responsible for the divergent structural and functional properties observed here, as well as the thermal stability of p23 and its truncation mutants. The association of the p23 β-sheet core with Hsp90, client proteins/interacting partners or small molecules, such as gedunin, should disturb the soft interaction of the p23 C-terminal tail on the β-sheet core, increasing the C-terminal dynamics which also may disrupt the amphipathic α-helix. Once the p23 C-terminal tail is released, it could allow additional interactions with the M-domain of Hsp90, or could act as a fly casting (1), recruiting interacting partners or even serve as a substrate for caspase cleavage (2), generating the p19 cleavage product, or serve as a substrate for phosphorylation (3).

Acknowledgments

CHIR, JCB and LRSB are CNPq Research Fellows and thank FAPESP – Brazil (2011/23110-0; 2012/50161-8) and CNPq – Brazil

for financial support. We thank the LNBio/CNPEM-ABTLuS (Campinas, Brazil) for making the AUC device available. We also thank the LNLS/CNPEM-ABTLuS (Campinas, Brazil) staff for use of the SAXS beamline.

Appendix A. Supplementary data

Supplementary data associated with this article can be found, in the online version, at http://dx.doi.org/10.1016/j.abb.2014.10.015.

References

[1] F.J. Echtenkamp, B.C. Freeman, in: W.A. Houry (Ed.), The Molecular Chaperones Interaction Networks in Protein Folding and Degradation, Springer New, York, 2014, pp. 207–232.
[2] J.L. Johnson, D.O. Toft, J. Biol. Chem. 269 (1994) 24989–24993.
[3] J.L. Johnson, T.G. Beito, C.J. Krco, D.O. Toft, Mol. Cell. Biol. 14 (1994) 1956–1963.
[4] J.L. Johnson, D.O. Toft, Mol. Endocrinol. 9 (1995) 670–678.
[5] S.J. Felts, D.O. Toft, Cell Stress Chaperon 8 (2003) 108–113.
[6] F.J. Echtenkamp, E. Zelin, E. Oxelmark, J.I. Woo, B.J. Andrews, M. Garabedian, B.C. Freeman, Mol. Cell 43 (2011) 229–241.
[7] T. Kobayashi, Y. Nakatani, T. Tanioka, M. Tsujimoto, S. Nakajo, K. Nakaya, M. Murakami, I. Kudo, Biochem. J. 381 (2004) 59–69.
[8] T. Tanioka, Y. Nakatani, N. Semmyo, M. Murakami, I. Kudo, J. Biol. Chem. 275 (2000) 32775–32782.
[9] R.V. Rao, K. Niazi, P. Mollahan, X. Mao, D. Crippen, K.S. Poksay, S. Chen, D.E. Bredesen, Cell Death Differ. 13 (2006) 415–425.
[10] G. Gausdal, B.T. Gjertsen, K.E. Fladmark, H. Demol, J. Vandekerckhove, S.O. Doskeland, Leukemia 18 (2004) 1989–1996.
[11] J. Mollerup, M.W. Berchtold, FEBS Lett. 579 (2005) 4187–4192.
[12] A.J. Weaver, W.P. Sullivan, S.J. Felts, B.A.L. Owen, D.O. Toft, J. Biol. Chem. 275 (2000) 23045–23052.
[13] T. Weikl, K. Abelmann, J. Buchner, J. Mol. Biol. 293 (1999) 685–691.
[14] F. Forafonov, O.A. Toogun, I. Grad, E. Suslova, B.C. Freeman, D. Picard, Mol. Cell. Biol. 28 (2008) 3446–3456.
[15] M.A. Martinez-Yamout, R.P. Venkitakrishnan, N.E. Preece, G. Kroon, P.E. Wright, H.J. Dyson, J. Biol. Chem. 281 (2006) 14457–14464.
[16] S. Bose, T. Weikl, H. Bugl, J. Buchner, Science 274 (1996) 1715–1717.
[17] B.C. Freeman, D.O. Toft, R.I. Morimoto, Science 274 (1996) 1718–1720.
[18] L. Neckers, J. Biosci. 32 (2007) 517–530.
[19] L.M. Gava, C.H.I. Ramos, Curr. Chem. Biol. 3 (2009) 10–21.
[20] V.C.H. da Silva, C.H.I. Ramos, J. Proteomics 75 (2012) 2790–2802.
[21] N.E. Simpson, W.M. Lambert, R. Watkins, S. Giashuddin, S.J. Huang, E. Oxelmark, R. Arju, T. Hochman, J.D. Goldberg, R.J. Schneider, L.F.L. Reiz, F.A. Soares, S.K. Logan, M.J. Garabedian, Cancer Res. 70 (2010) 8446–8456.
[22] J.C. Young, F.U. Hartl, EMBO J. 19 (2000) 5930–5940.
[23] B. Panaretou, G. Siligardi, P. Meyer, A. Maloney, J.K. Sullivan, S. Singh, S.H. Millson, P.A. Clarke, S. Naaby-Hansen, R. Stein, R. Cramer, M. Mollapour, P. Workman, P.W. Piper, L.H. Pearl, C. Prodromou, Mol. Cell 10 (2002) 1307–1318.
[24] K. Richter, S. Walter, J. Buchner, J. Mol. Biol. 342 (2004) 1403–1413.
[25] M.M.U. Ali, S.M. Roe, C.K. Vaughan, P. Meyer, B. Panaretou, P.W. Piper, C. Prodromou, L.H. Pearl, Nature 440 (2006) 1013–1017.
[26] C.E. Stebbins, A.A. Russo, C. Schneider, N. Rosen, F.U. Hartl, N.P. Pavletich, Cell 89 (1997) 239–250.
[27] J. Hohfeld, D.M. Cyr, C. Patterson, EMBO Rep. 2 (2001) 885–890.
[28] L.H. Pearl, C. Prodromou, Adv. Protein Chem. 59 (2002) 157–186.
[29] S.P. Bohen, Mol. Biol. Cell 18 (1998) 3330–3339.
[30] I. Grad, T.A. McKee, S.M. Ludwig, G.W. Hoyle, P. Ruiz, W. Wurst, T. Floss, C.A. Miller, D. Picard, Mol. Cell. Biol. 26 (2006) 8976–8983.
[31] O.A. Toogun, W. Zeiger, B.C. Freeman, Proc. Natl. Acad. Sci. U.S.A. 104 (2007) 5765–5770.
[32] S.H. Woo, S. An, H.C. Lee, H.O. Jin, S.K. Seo, D.H. Yoo, K.H. Lee, C.H. Rhee, E.J. Choi, S.I. Hong, I.C. Park, J. Biol. Chem. 284 (2009) 30871–30880.
[33] K. Tosoni, A. Costa, S. Sarno, Mol. Cell. Biochem. 356 (2011) 245–254.
[34] K. Poksay, S. Banwait, D. Crippen, X. Mao, D. Bredesen, R. Rao, J. Mol. Neurosci. (2011) 1–12.
[35] C.A. Patwardhan, A. Fauq, L.B. Peterson, C. Miller, B.S.J. Blagg, A. Chadli, J. Biol. Chem. 288 (2013) 7313–7325.
[36] G. Deleage, C. Combet, C. Blanchet, C. Geourjon, Comput. Biol. Med. 31 (2001) 259–267.
[37] R. Elble, Biotechniques 13 (1992) 18–20.
[38] K.R. Oldenburg, K.T. Vo, S. Michaelis, C. Paddon, Nucleic Acids Res. 25 (1997) 451–452.
[39] E.S. Kroll, K.M. Hyland, P. Hieter, J.J. Li, Genetics 143 (1996) 95–102.
[40] V.V. Kushnirov, Yeast 16 (2000) 857–860.
[41] D.H.A. Corrêa, C.H.I. Ramos, Afr. J. Biochem. Res. 3 (2009) 164–173.
[42] P. Schuck, Biophys. J. 78 (2000) 1606–1619.
[43] J.C. Borges, C.H.I. Ramos, Curr. Med. Chem. 18 (2011) 1276–1285.
[44] P.V. Konarev, V.V. Volkov, A.V. Sokolova, M.H.J. Koch, D.I. Svergun, J. Appl. Crystallogr. 36 (2003) 1277–1282.
[45] A.V. Semenyuk, D.I. Svergun, J. Appl. Crystallogr. 24 (1991) 537–540.
[46] D.I. Svergun, J. Appl. Crystallogr. 25 (1992) 495–503.
[47] N. Blom, S. Gammeltoft, S. Brunak, J. Mol. Biol. 294 (1999) 1351–1362.
[48] J.V. Olsen, B. Blagoev, F. Gnad, B. Macek, C. Kumar, P. Mortensen, M. Mann, Cell 127 (2006) 635–648.
[49] S.H. McLaughlin, F. Sobott, Z.P. Yaol, W. Zhang, P.R. Nielsen, J.G. Grossmann, E.D. Laue, C.V. Robinson, S.E. Jackson, J. Mol. Biol. 356 (2006) 746–758.
[50] G.E. Karagoz, A.M.S. Duarte, H. Ippel, C. Uetrecht, T. Sinnige, M. van Rosmalen, J. Hausmann, A.J.R. Heck, R. Boelens, S.G.D. Rudiger, Proc. Natl. Acad. Sci. U.S.A. 108 (2011) 580–585.
[51] T. Trudeau, R. Nassar, A. Cumberworth, E.T. Wong, G. Woollard, J. Gsponer, Structure 21 (2013) 332–341.
[52] D. Song, L.s. Li, P.R. Arsenault, Q. Tan, A.W. Bigham, K.J. Heaton-Johnson, S.R. Master, F.S. Lee, J. Biol. Chem. (2014).